Journal of Thermal Analysis and Calorimetry, Vol. 80 (2005) 131–136

INFLUENCE OF $CaCO_3$ NANOPARTICLES SHAPE ON THERMAL AND CRYSTALLIZATION BEHAVIOR OF ISOTACTIC POLYPROPYLENE BASED NANOCOMPOSITES

M. Avella[*], *S. Cosco, M. L. Di Lorenzo, E. Di Pace and M. E. Errico*

Istituto di Chimica e Tecnologia dei Polimeri (CNR), c/o Comprensorio Olivetti, Via Campi Flegrei, 34, 80078 Pozzuoli (NA), Italy

The influence of calcium carbonate nanoparticles with different shapes (spherical and elongated) on the thermal properties and crystallization behavior of isotactic polypropylene was investigated. $CaCO_3$ nanoparticles were covered by an appropriate coating agent to improve the interfacial adhesion between the filler and the polyolefin matrix. The nanocomposites were prepared by melt mixing and subsequent compression molding. A remarkable effect of $CaCO_3$ on the thermal properties of iPP was observed. Moreover, the analysis of crystallization kinetics showed that $CaCO_3$ nanopowder coated with PP-MA are efficient nucleating agents for iPP, and the overall crystallization rate results higher than plain iPP.

Keywords: *calcium carbonate nanopowder, crystallization, nanocomposites*

Introduction

The recent developments of new materials based on nanometer sized filler particles in polymeric matrices represent a radical alternative to conventional microfilled polymers or polymer blends, resulting in a disruptive change in composite technology [1–5]. As well known, nanocomposite properties are strongly influenced by the nature and extent of the interface, hence a large surface to volume ratio of the filler allows to largely improve material properties [6].

The key factors for the preparation of enhanced performance nanomaterials are to obtain a homogeneous distribution of the nanoparticles within the polymer matrix, and to promote a strong interfacial adhesion between the matrix and the nanofiller. Uniform dispersion of the nanometer particles offers a major specific surface area enhancement, compared to conventional reinforcements of micrometer size. As a result, significantly smaller amounts of filler (1–6 mass%), compared to conventional composites (10–50 mass%), can induce dramatic changes in host matrix properties.

Among the ceramic nanoparticles, layered silicates, such as montmorillonite, have been extensively studied in recent years, due to their large aspect ratio [7–9]. Other types of fillers have been utilized as well. Among them, calcium carbonate in micrometric dimensions (1–50 μm) is also one of most commonly used inorganic filler for thermoplastics. Previous studies have demonstrated that the use of $CaCO_3$ nanoparticles, when coated with appropriate coupling agents, can lead to the achievement of polymer-based nanocomposites with improved properties with respect to the conventional microcomposites, including mechanical, thermal and wear properties [10–14].

Another important parameter that can affect the final properties of the nanocomposites is the shape of the $CaCO_3$ nanoreinforcement: the use of either spherical or elongated nanoparticles is expected to differently influence many physical properties of the final nanocomposites, such as permeability, thermal and mechanical behavior, etc.

In this communication, results on thermal and crystallization behavior of isotactic polypropylene (iPP) filled with calcium carbonate ($CaCO_3$) nanoparticles are presented. In particular, $CaCO_3$ nanoparticles coated with a polypropylene-*co*-maleic anhydride graft copolymer (PP-MA) as a coupling agent [15], and characterized by different shapes (spherical and elongated) have been selected as reinforcing phase.

Experimental

Materials

Isotactic polypropylene (iPP) was a commercial product, Moplen X 30 S, kindly supplied by Basell Polyolefins (Ferrara, Italy). It has M_n=4.69·10^4 g mol^{-1}, M_w=3.5·10^5 g mol^{-1} and M_z=2.06·10^6 g mol^{-1}.

Calcium carbonate nanoparticles, emulsion-coated with a graft copolymer, isotactic polypropylene-*co*-maleic anhydride, were kindly supplied by Solvay Advanced Functional Minerals (France). Two types of

* Author for correspondence: mave@ictp.cnr.it

1388–6150/$20.00

Akadémiai Kiadó, Budapest, Hungary
Springer, Dordrecht, The Netherlands

$CaCO_3$ nanofillers, with different aspect ratio, were used: spherical and elongated.

Literature data indicate that $CaCO_3$ nanopowder does not undergo degradation phenomena at the temperatures used for melt mixing and crystallization analyses of the nanocomposites [16].

Preparation of ceramic nanocomposites

iPP/$CaCO_3$ nanocomposites were obtained by mixing the components in a Brabender-like apparatus (Rheocord EC of HAAKE Inc., New Jersey, USA) at 200°C and 32 rpm for 10 min. The mixing ratios of iPP/$CaCO_3$ (mass/mass) were: 100/0, 99/1, 97/3.

Plain iPP and iPP/$CaCO_3$ nanocomposites were compression-molded in a heated press at 200°C for 2 min without any applied pressure. After this period, a pressure of 100 bar was applied for 3 min, then the press platelets, containing coils for fluids, were rapidly cooled to room temperature by cold water. Finally, the pressure was released and the mold removed from the plates.

Electron microscopy

Morphological analysis of $CaCO_3$ nanoparticles was conducted by scanning electron microscopy (SEM) using a Philips XL 20 series microscope. Before the electron microscopy observation, the surfaces were coated with Au–Pd alloy with a SEM coating device (SEM Coating Unit E5150 – Polaron Equipment Ltd.).

Calorimetry

The thermal properties were measured with a differential scanning calorimeter Mettler DSC-30. The apparatus was calibrated with pure indium, lead and zinc standards at various scanning rates. Dry nitrogen gas with a flow rate of 20 mL min^{-1} was purged through the cell during all measurements and thermal treatments.

Bulk crystallization kinetics of iPP/$CaCO_3$ nanocomposites was analyzed in non-isothermal conditions. The samples were heated from 30 to 190°C at a scanning rate of 20 K min^{-1}, kept at this temperature for 2 min, then cooled to room temperature at four different scanning rates: 1, 2, 4 and 8 K min^{-1}, then heated at 20°C min^{-1}. Dry nitrogen gas with a flow rate of 20 mL min^{-1} was purged through the cell.

The melting temperatures (T_m) were measured as the minima of the endothermic peaks of DSC traces. The crystalline fractions (X_c) were calculated by integration of the melting endotherms, using the literature data for the enthalpy of fusion of iPP in the fully crystalline state of 210 J g^{-1} [13].

Thermogravimetry

The thermal stability of the samples was measured by means of thermogravimetrical analysis (TG) with a TC 10A Mettler TG equipped with a M3 analytical thermobalance, by recording the mass loss as a function of temperature. Each sample was heated from 40 to 600°C at a scanning rate of 10 K min^{-1} in air atmosphere. The degradation temperature (T_d) was taken as the temperature corresponding to 50% loss of the initial mass.

Dynamic-mechanical analysis

Dynamic-mechanical data (DMTA) were collected at 1 Hz and at a heating rate of 3 K min^{-1} from –50 to 160°C under nitrogen with a Dynamic Mechanical Thermal Analyser MK III, Polymer Laboratories, configured for automatic data acquisition. The experiments were performed in bending mode.

Optical microscopy

Spherulite growth rates were determined by optical microscopy, using a Zeiss polarizing microscope equipped with a Linkam TMHS 600 hot stage. A small piece of each sample was squeezed between two microscope slides, then inserted in the hot stage. The thermal treatments before isothermal crystallization were identical to those used for the analysis of bulk crystallization rates. iPP/$CaCO_3$ samples were heated from 30 to 190°C at a rate of 20 K min^{-1}, melted at 190°C for 3 min, cooled at a rate of 50 K min^{-1} to the selected crystallization temperature (T_c) and allowed to isothermally crystallize. The radius of the growing crystals was monitored by taking photomicrographs at appropriate intervals of time, using a JVC TK-1085E Video Camera coupled with the software Image-Pro Plus 3.0. Dry nitrogen was used as purge gas in the hot stage during all measurements and thermal treatments.

Results and discussion

Nanoparticles

In order to determine the morphology of the nanosized powder samples, the $CaCO_3$ nanoparticles were analyzed as received by scanning electron microscopy (SEM). The electron micrographs of the two fillers are presented in Fig. 1. For both the samples the nanoparticles have some tendency to form aggregates, whose dimensions are higher than those of the isolated particles. Formation of the aggregates is enhanced by the polymeric coating (isotactic polypropylene grafted with maleic anhydride). The presence of the coating also

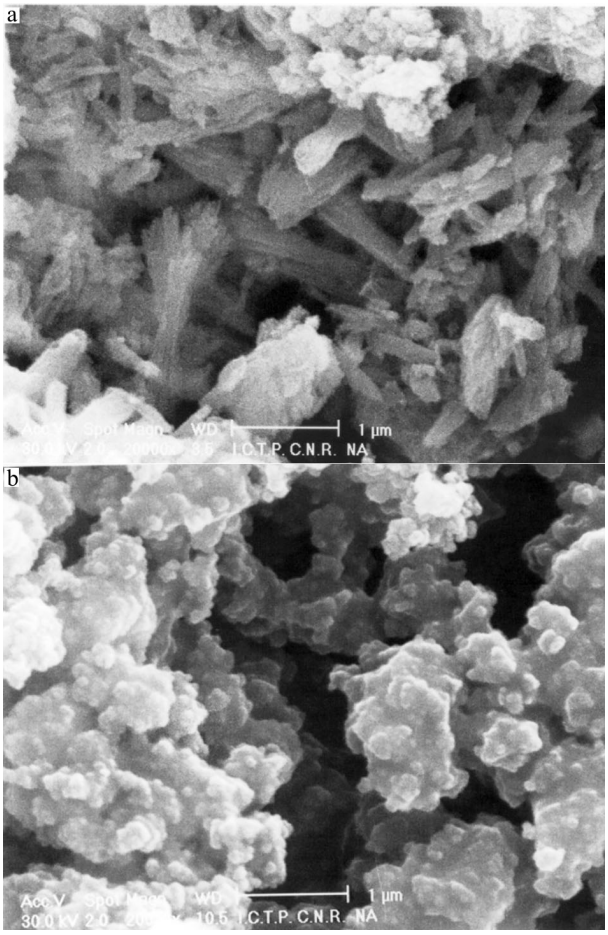

Fig. 1 Electron micrographs of the $CaCO_3$ ceramic nanopowder: a – Type-F $CaCO_3$; b – Type-S $CaCO_3$

complicates the morphological analysis of the nanosized particles, as surface details become difficult to resolve.

The electron micrographs evidence the different morphology and aspect ratio of the fillers. Figure 1a shows a large aggregate of elongated $CaCO_3$ nanoparticles. The nanoparticles have a length of about 1 μm, and lateral dimensions ranging from 50 to 150 nm. The $CaCO_3$ filler illustrated in Fig. 1a will be denoted as 'E' (elongated) throughout the article. The second type of $CaCO_3$ nanopowders, shown in Fig. 1b, have a spherical appearance, with diameter ranging from 40 to 70 nm. These nanoparticles will be denoted as 'S' (spherical).

Thermal properties of compression-molded iPP/$CaCO_3$ nanocomposites

The thermal stability of iPP and iPP-based nanocomposites was analyzed with thermogravimetry. The values of the degradation temperature (T_d), that corresponds to 50% loss of initial mass, are presented in the second column of Table 1. The presence of

Table 1 Thermal parameters of iPP and iPP/$CaCO_3$ nanocomposites: decomposition temperature (T_d), and glass transition temperature (T_g)

Sample	T_d/°C	T_g/°C
iPP	368	20
iPP+1% S	382	26
iPP+3% S	378	22
iPP+1% E	390	24
iPP+3% E	391	26

nanoparticles raises the degradation temperature of the material of about 20–25°C, the increase being slightly more marked for the nanocomposite containing the elongated $CaCO_3$ filler.

Results of DMTA tests are illustrated in Fig. 2. Two major transitions can be evidenced for each sample. The first maximum in the tanδ *vs*. temperature plot, centered around 20–25°C, is due to the glass transition (T_g) of the mobile amorphous phase (MAP) of iPP, the second, broader, transition around 80°C is attributed to T_g of the rigid amorphous phase (RAP) of iPP [18]. Due to the broadness of the transition, no influence of $CaCO_3$ on T_g of the RAP can be deduced from the DMTA curves of Fig. 2. Conversely, some effects of $CaCO_3$ on T_g of MAP of iPP can be observed, as summarized in the third column of Table 1. The T_g of plain iPP is 20°C, in agreement with data [19], whereas higher values were observed for the reinforced samples. Increases of both the glass transition and the degradation temperature in the presence of a rigid filler into the polymeric matrix, are commonly observed in ceramic nanocomposites [20]. These increases arise from the strong interconnection and good adhesion between the two phases, which reduces the mobility of polypropylene chains, when nanoparticles with a very high interfacial area are homogeneously dispersed into the polymer matrix [21].

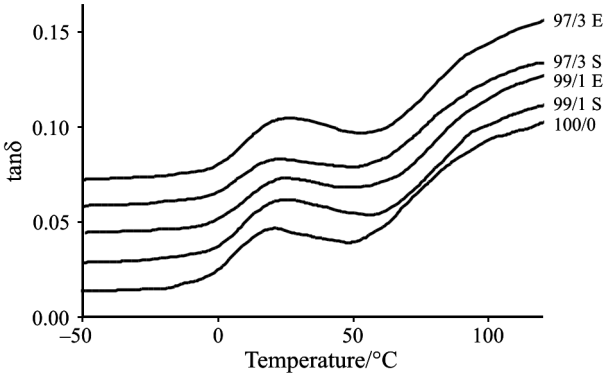

Fig. 2 Tanδ curves of iPP/$CaCO_3$ nanocomposites

Crystallization kinetics

The radial growth rates (G) of iPP spherulites as a function of crystallization temperature are reported in Fig. 3 for plain iPP and for the nanocomposites with different composition. The addition of 3% of $CaCO_3$ causes a very light decrease of the rate of spherulite growth, compared to plain polypropylene, although the difference is quite close to the experimental uncertainty. When 1% of nanosized $CaCO_3$ is added to iPP, no remarkable effect on G is observable in the explored temperature range.

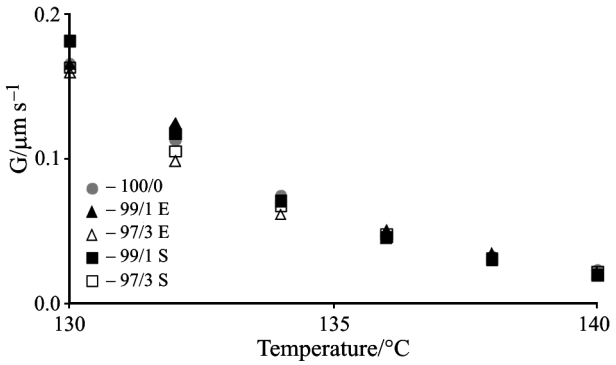

Fig. 3 Spherulite growth rates of iPP/$CaCO_3$ nanocomposites

The addition of a second component to a crystallizable polymer often produces a decrease of the rate of spherulite growth [22]. This decrease is caused by the need to reject, occlude and/or deform the dispersed particles, which results in an increase of the energy barriers to crystal growth. These energy barriers, that have been quantified for a few polymer-filler pairs [22–24], are generally quite small, and depend on a series of parameters, including the amount and the dimension of the filler, as well as on the rate of spherulite growth at a given temperature [24]. In several cases, it has also been reported that the presence of dispersed particles in binary non-miscible blends or composites has no effect on the measured value of G [22]. The very small size of the $CaCO_3$ used, coupled with its small amount in the nanocomposites, produces only a very minor effect on the rate of growth of polypropylene spherulites, which is slightly detectable only when at least 3% of $CaCO_3$ is added to iPP.

The bulk crystallization kinetics of iPP and the nanocomposites was analyzed in dynamic conditions, by cooling the samples from the melt at various scanning rates. The influence of the filler on dynamic solidification of iPP is shown in Fig. 4, which presents the thermoanalytical curves of iPP and iPP/$CaCO_3$ nanocomposites crystallized at χ=8 K min^{-1}. Similar trends were obtained also for the other cooling rates. From the solidification exotherms, the onset (T_b) and peak (T_p) temperatures were measured, and are shown in Fig. 5.

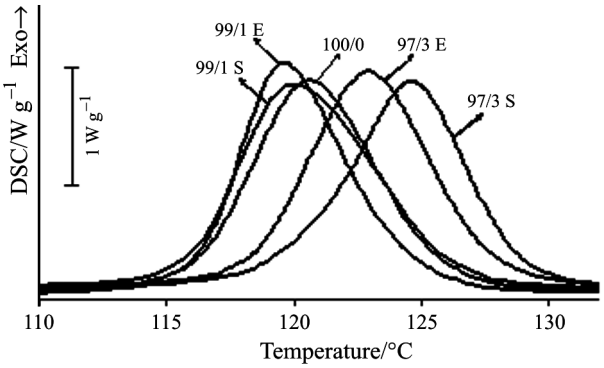

Fig. 4 DSC thermoanalytical curves of iPP/$CaCO_3$ nanocomposites at various compositions, measured during cooling from the melt at 8 K min^{-1}

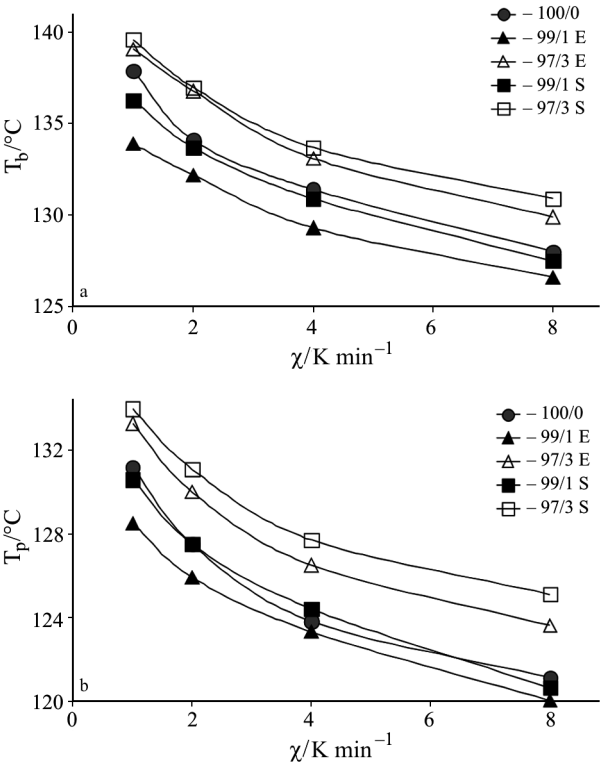

Fig. 5 a – Onset and b – peak temperatures of crystallization of iPP/$CaCO_3$ nanocomposites at various cooling rates

Both T_b and T_p values depend on cooling rate and composition. For every sample, with increasing the cooling rate, χ, the crystallization curves shift to lower temperatures, as typical for polymer crystallization: at lower χ there is more time to overcome the energy barriers for nucleation, so crystallization starts at higher temperatures, whereas at higher χ the nuclei become active at lower temperatures [25].

In polymer samples containing added foreign particles, the temperature at which crystallization starts is indicative of the effectiveness of the filler to

promote heterogeneous nucleation [26]. The addition of 3% $CaCO_3$ induces crystallization to start at high temperatures compared to plain iPP. When only 1% $CaCO_3$ is present, the onset of phase transition is slightly retarded, indicating that a minimum amount of nanosized $CaCO_3$ is needed to for an effective ability to nucleate iPP crystals. The efficiency of a nucleating agent depends on a number of factors. Changes in surface chemistry of the filler influences the behavior significantly, because of the interactions between the polymer matrix and the coating, as demonstrated by a series of experiments conducted by Ribnikář on isotactic polypropylene reinforced with a series of calcite fillers characterized with different types of coating [27]. In the case of $CaCO_3$ coated with PP-MA, the efficiency as nucleating agent is enhanced by the presence of PP-MA, which can also crystallize, facilitating the attachment of crystallizing iPP chains onto the $CaCO_3$ surface. Morphology and dimensions of the filler also have a dramatic on the ability to start polymer crystallization.

The melting behavior of the nanocomposites, analyzed by DSC after dynamic crystallization, was found to be unaffected by the presence of $CaCO_3$: for a same cooling rate, both melting temperature and enthalpy were identical for plain iPP and 1 and 3% iPP/$CaCO_3$ nanocomposites. No differences in melting temperature of iPP spherulites after isothermal crystallization were also observed by optical microscopy. As primary crystallization upon cooling occurs at different temperatures for the various iPP/$CaCO_3$ compositions, as shown in Figs 4 and 5, an influence of composition on fusion behavior might be expected [28]. However, it is likely that the large reorganization of iPP crystals occurring during the heating scan that leads to fusion, masks the differences in the thermal stability of the crystals that were formed upon primary crystallization, resulting in a constant melting point with $CaCO_3$ content [25].

To analyze the kinetics of the non-isothermal crystallization process, the method proposed by Ozawa [30] was applied. According to Ozawa, the degree of conversion at temperature T is related to the cooling rate χ by the expression:

$$X(T) = 1 - e^{-\frac{k(T)}{\chi^n}} \quad (1)$$

where $X(T)$ is the relative crystallinity at temperature T, n is the Avrami exponent, and $k(T)$ is the cooling crystallization function. Equation (1) can be rewritten as:

$$\log\{-\ln[1-X(T)]\} = \log[k(T)] - n\log\chi \quad (2)$$

By plotting the left term of Eq. (2) *vs*. logχ, a straight line should be obtained and the kinetic parameter n can be derived from its slope. Previous investigations showed that this method can be applied to analyze the dynamic solidification of plain iPP [31]. The

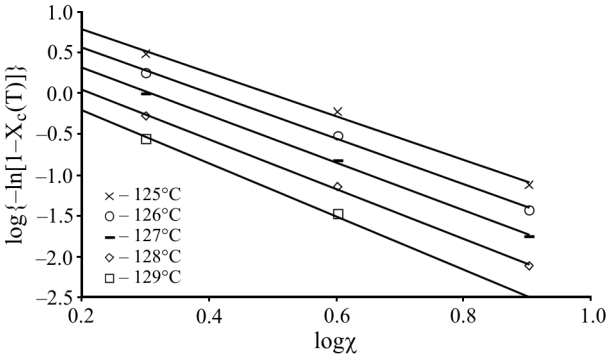

Fig. 6 Ozawa plot of iPP-$CaCO_3$ nanocomposite with 1% of type-E $CaCO_3$ filler

log{–ln[1–$X(T)$]} *vs*. logχ plots is exhibited in Fig. 6 for a representative iPP/$CaCO_3$ composition. Similar plots were obtained for the other iPP/$CaCO_3$ compositions. Experimental data for plain iPP and the iPP/$CaCO_3$ nanocomposites were fitted by straight lines, showing that Ozawa equation can be successfully applied to describe the non-isothermal crystallization behavior of iPP also in the presence of $CaCO_3$. For all the analyzed samples, the Ozawa exponent is about 3, as often reported for iPP [28, 31], indicating heterogeneous nucleation and tridimensional growth of iPP crystals. Morphological investigations conducted by optical microscopy confirmed the conclusions derived from Ozawa analysis.

Conclusions

The thermal properties of isotactic polypropylene can be varied upon addition of nanosized $CaCO_3$ particles. The coating with iPP-MA facilitates the establishment of interactions between the nanoparticles and the polyolefin matrix, resulting in good adhesion level.

The addition of $CaCO_3$ causes an increase in the glass transition temperature and a better thermal stability of the material. The presence of the nanofiller also induces crystallization to start at higher temperatures when at least 3% $CaCO_3$ is added to iPP. The different aspect ratio of the two types of $CaCO_3$ particles used is responsible for the diverse effect of calcium carbonate particles on crystallization of iPP, mainly because of the different specific surface of the filler in contact with the polymer matrix.

Acknowledgements

The authors are very grateful to Dr. Karine Cavalier of Solvay Advanced Functional Minerals (France) for kindly providing the $CaCO_3$ nanoparticles, as well as for useful discussions.

Financial support of Regione Campania, LR 28/5/02 n. 5, is gratefully acknowledged.

References

1 H. Schmidt, J. Non-Cryst. Solids, 73 (1985) 681.
2 D. R. Ulrich, J. Non-Cryst. Solids, 121 (1990) 465.
3 B. M. Novak, Adv. Mater., 5 (1993) 422.
4 B. M. Novak, Adv. Mater., 5 (1993) 839.
5 J. E. Mark, Polym. Eng. Sci., 36 (1996) 2905.
6 C. Sanchez and F. Ribot, New J. Chem., 18 (1994) 1007.
7 W. B. Xu, Z. F. Zhou, M. L. Ge and W. P. Pan, J. Therm. Anal. Cal., 78 (2004) 91.
8 W. B. Xu, H. B. Zhai, H. Y. Guo, Z. F. Zhou, N. Whitely and W. P. Pan, J. Therm. Anal. Cal., 78 (2004) 101.
9 S. Y. Moon, J. K. Kim, C. Nah and Y. S. Lee, Eur. Polym. J., 40 (2004) 1615.
10 C. M. Chan, J. Wu, J. X. Li and Y. K. Cheung, Polymer, 43 (2002) 2981.
11 W. C. J. Zuiderduin, C. Westzaan, J. Huétink and R. J. Gaymans, Polymer, 44 (2003) 261.
12 Z. Bartczak, A. S. Argon, R. E. Cohen and M. Weinberg, Polymer, 40 (1999) 2347.
13 G. Levita, A. Marchetti and A. Lazzeri, Polym. Compos., 10 (1989) 39.
14 M. L. Di Lorenzo, M. Avella and M. E. Errico, J. Mater. Sci., 37 (2002) 2351.
15 M. L. Di Lorenzo and M. Frigione, J. Polym. Eng., 17 (1997) 429.
16 D. R. Lide, Ed., Handbook of Chemistry and Physics, 76th Ed., CRC Press, Boca Raton, FL 1995.
17 ATHAS Data Bank, http://web.utk.edu/~athas/databank/intro.html Ed. M. Pyda, (1994).
18 B. Wunderlich, Progr. Polym. Sci., 28 (2003) 383.
19 S. Cimmino, E. D'Alma, M. L. Di Lorenzo, E. Di Pace and C. Silvestre, J. Polym. Sci., Part B: Polym. Phys., 37 (1999) 867.
20 B. J. Briscoe, in Friction and Wear of Polymer Composites, Vol. 1, K. Friedrich Ed., Composite Materials Series, R. B. Pipes Series Ed., Elsevier, Amsterdam 1986, p. 31.
21 M. Avella, M. E. Errico, S. Martelli and E. Martuscelli, Appl. Organomet. Chem., 15 (2001) 1.
22 M. L. Di Lorenzo, Progr. Polym. Sci., 28 (2003) 663.
23 E. Martuscelli, Polym. Eng. Sci., 24 (1984) 563.
24 Z. Bartczak, A. Gałęski and E. Martuscelli, Polym. Eng. Sci., 24 (1984) 1155.
25 M. L. Di Lorenzo and C. Silvestre, Progr. Polym. Sci., 24 (1999) 917.
26 L. C. López and G. L. Wilkens, Polymer, 30 (1989) 882.
27 F. Ribnikář, J. Appl. Polym. Sci., 42 (1991) 2727.
28 B. Wunderlich, Macromolecular Physics, Vol. 2: Crystal Nucleation, Growth, Annealing, Academic Press, New York 1976.
29 B. Wunderlich, Macromolecular Physics, Vol. 3, Crystal Melting, Academic Press, New York 1980.
30 T. Ozawa, Polymer, 12 (1971) 150.
31 M. L. Di Lorenzo, S. Cimmino and C. Silvestre, J. Appl. Polym. Sci., 82 (2001) 358.